International Forum on Aeroelasticity and Structural Dynamics
IFASD 2019
9-13 June 2019, Savannah, Georgia, USA

THERMAL CORRECTION OF STRAIN GAGE MEASUREMENTS ON FLEXIBLE X-HALE AIRCRAFT

Jéssica S. Martins[1], Flávio L. S. Bussamra[1], Juliano A. Paulino[1], Antônio B. Guimarães Neto[1]

[1]Instituto Tecnológico de Aeronáutica
São José dos Campos, SP, 12228-900, Brazil
jsantosmartins93@gmail.com

Keywords: embedded strain gage, flexible aircraft, thermal correction

Abstract: The development of modern, more efficient transport aircraft and High-Altitude-Long-Endurance (HALE) aircraft requires solutions that involve lightweight structures and high aspect ratio wings for maximum aerodynamic efficiency. However, this may result in flexible wings, such that the coupling between rigid-body and structural modes deteriorates stability and handling qualities of the aircraft. These can be improved by the continuous operation of control systems with the use of structural information, such as wing deformed shape. Strain gages can be used for such an application. However these sensors may have input interference, such as temperature variation, that can cause false strain responses other than the expected measurements due to flight loads. This work presents the analyzes of strain gage measurements due to thermal loads in the X-HALE aircraft wing. Three thermal correction methods were proposed: functions of temperature, dummy gage, and high-pass filtering. Each was tested on indoor and outdoor experiment setup, which uses a lamp and natural temperature variation throughout a full day as heat sources. All methods were effective in removing thermal drift of indoor experiment data. However, only high-pass filtering method was successful in the outdoor experiment. Indoor thermal test results done on the full 4m X-HALE aircraft, with the addition of impact excitations on the aircraft's wing tip, showed that the high-pass filtering was able to remove thermal drift while maintaining all responses in the frequency range of interest. Therefore, this method is suitable to the present application.

1 INTRODUCTION

According to the Prandtl's lifting-line theory, induced drag of a lift surface is inversely proportional to its aspect ratio (AR). Since the reduction of drag allows for an increase of aerodynamic efficiency [1], lightweight high aspect ratio aircraft have been of interest for applications such as environmental detection and military reconnaissance [2]. However, structural requirements limit the AR. Increasing the elongation results in increased flexibility, considering that the structural mass is the same. This in turn can significantly modify the aircraft's flying qualities, or adversely affect aeroelastic stability making the control of high-altitude long-endurance aircraft (HALE) a challenge to this day.

In an effort to obtain experimental data for flexible aircraft model validation, Cesnik and collaborators designed the X-HALE aircraft [3], which is a wing-boom-tail type aircraft with AR = 20, 30 and 40 for the four-meter-, six-meter-, and eight-meter-span configurations. Instituto Tecnológico de Aeronáutica (ITA), as part of the Advanced Studies in Flight Physics project,

Figure 1: 4m X-HALE aircraft in flight, at the São José dos Campos Professor Urbano Ernesto Stumpf Airport, on December 07^{th}, 2017.

built two different versions of this aircraft: X-HALE aircraft with 4m and 6m of wing span. Flight tests are currently being done on the 4m aircraft (Fig. 1). Meanwhile, the 6m X-HALE aircraft is being constructed with the addition of embedded strain gages in four of the six wing modules. These strain gages will measure bending, shear and torsion in real time during flight tests, that will be used as input data in control systems. Continuous operation of control systems is of interest in this second configuration of X-HALE aircraft because of its high AR and flexibility. These factors deteriorates the aircraft handling qualities, since the deformed state of the wing modifies the vibration modes and their couplings [4].

Strain gage sensors may have input interference during data acquisition other than the expected measurements due to flight loads (aerodynamic loads, inertial loads, etc). Temperature variations, for example, cause thermal strain (thermal drift) [5] that can be minimized by selecting low STC value (Self Temperature Compensated) strain gages compatible with substrate material thermal expansion and by using full Wheatstone strain gage bridges. However, in some cases these measures are not enough to reduce thermal drift to magnitudes that can be neglected. For those cases, thermal corrections are recommended.

The measured strain $\varepsilon\left(\Delta T\right)$ is given by the sum of stress-induced strain $\varepsilon_{\sigma}\left(\Delta T\right)$ and apparent strain due to thermal load $\varepsilon_{app}\left(\Delta T\right)$ that is defined by

$$\varepsilon_{app}\left(\Delta T\right) = \left[\left(\alpha_s - \alpha_g\right) + \frac{\gamma}{k}\right] \Delta T \tag{1}$$

where ΔT is a uniform substrate temperature change, α_s and α_g are the substrate and strain gage thermal expansion coefficients, γ is the temperature coefficient of resistivity and k is the gage factor. When strain gage and substrate are subjected to ΔT, each attempts to expand/contract according to their own thermal expansion coefficient. However, strain gage and substrate are bonded together, therefore, the substrate (with greater stiffness) imposes its expansion to the strain gage. An additional strain of $\left(\frac{\gamma}{GF}\right)\Delta T$ will be measured by strain gage sensors [6] which is not related to the mechanical loads. Thermal corrections have the main goal to remove $\varepsilon_{app}\left(\Delta T\right)$ from the sensors measurement.

2 OBJECTIVE

The main goal of the current work is to propose a method to obtain strain measurements, with thermal correction, in real-time, suitable to be used as feedback signal for automatic control in

the X-HALE aircraft.

To achieve this goal, the following steps were accomplished: determine the base noise of strain gage sensors embedded between composite layers of X-HALE wing module; analyze responses of bending, shear and torsion full strain gage embedded bridges when under thermal loads; test functions of temperature, dummy gage and high-pass filtering thermal correction methods; and compare the correction results to determine witch is more suitable for application in X-HALE aircraft.

3 METHODOLOGY

The X-HALE aircraft consists of 1m wing modules connected to booms with horizontal tails attached and pods with motors, propellers, batteries, and processor boards. The X-HALE wing box is a foam base covered by fiber glass Henkel Pre-preg Epoxy-glass120/F155 with layer thickness of 0.12 mm and layup $[90_5]$ in relation to the x axis of Figs. 2 and 3. The 6^{th} composite layer creates the airfoil shape with dimension according to Jones [7].

Strain gages CEA 06-250-UW-350 for bending and CEA 06-187-UV-350 for shear and torsion Wheatstone bridges were positioned on top of the 5^{th} fiber layer, as depicted in Fig. 2 and 3. Bending and shear bridges are positioned 50 cm from the wing module edge in relation to wing span, while torsion bridge is positioned 55 cm from it.

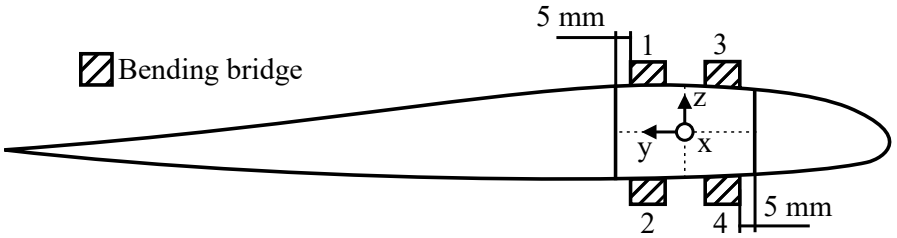

Figure 2: Bending strain gages positions on X-HALE wing module.

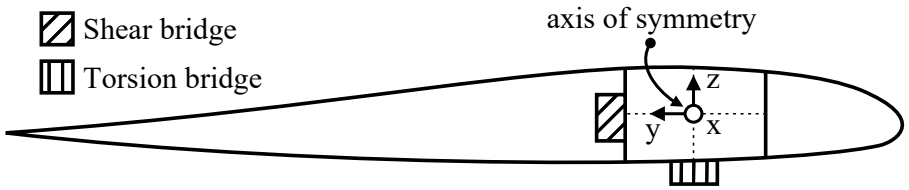

Figure 3: Shear and torsion strain gages positions on X-HALE wing module.

Two LM35 temperature sensors were attached to top and bottom wing surface near top and bottom bending strain gage and a third temperature sensor was positioned inside the wing box near shear strain gages. They will be called T_{Top}, T_{Base} and T_{Center} temperature sensors from now on. These positions were chosen in order to measure the temperature that each strain gage where subjected to during the experiment. T_{Top} and T_{Base} temperature sensors were covered with a thin styrofoam layer in order to protect them from heat coming straight from the heat source.

Two CEA 06-250-UW-350 strain gages were used as dummy gages and were positioned near T_{Top} and T_{Base} temperature sensors. They will be called D_{top} and D_{base} from now on. Both were kept free to expand and contract between two plastic sheets that were loosely attached to wing surface.

The data acquisition system (DAQ) was based on Arduino MEGA 2560 platform, with 10-bit

resolution and sampling rate ranging from 1 Hz to 100 Hz, according to each test requirement. Signal conditioning was made by ICA5 S strain gauge analog amplifiers.

3.1 Experiments

3.1.1 Stability Over Time Test

Bending, shear and torsion strain were measured for 3 hours with minimum system disturbance (such as vibration and temperature changes) and no load application. This was done in order to determine how stable and reliable strain gage measurements of embedded bridges are with time and to measure the sensors base noise. This test was done on the bi-supported configuration presented in Fig. 4 in the 1 m wing module. The supports used had the same shape as the lower surface of the wing.

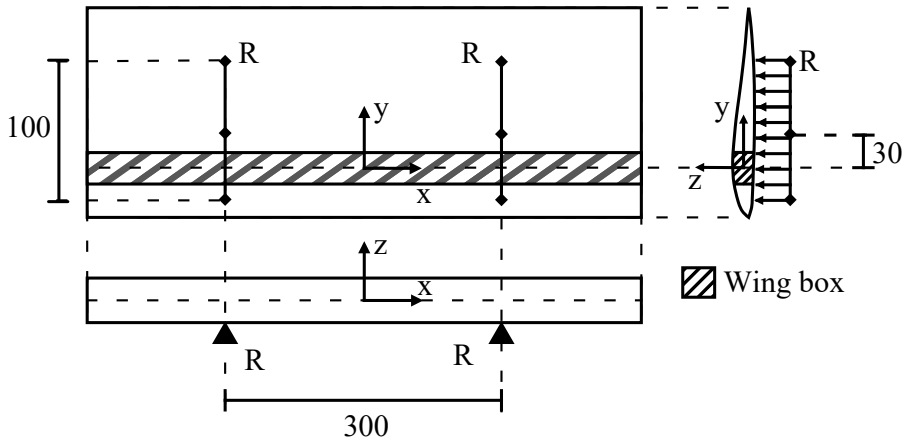

Figure 4: Bi-supported configuration in 1 m X-HALE wing module.

Based on this data, a Moving Average Filter (MAF) with average of 50 data points was implemented. The sampling rate was equal to 1 Hz in every measurement for which the MAF was used. This filter was used with the only objective of noise reduction so that the thermal responses could more easily be observed.

3.1.2 Indoor Thermal Experiment

This experiment used 120W 220V halogen lamp as heat source, and dummy gages, temperature sensors and embedded strain gages as sensors. The lamp was connected to a dimmer in order to adjust the light intensity during experiment. Three tests were conducted with 3 different lamp voltages in order to test the thermal drift on strain gage sensors due to different thermal loads. This slightly changed the heating hate and maximum temperature achieved on each test. These tests are called tests 1, 2 and 3 in ascending lamp voltage order. They were all done on the bi-supported configuration on the 1 m wing module with sampling rate of 1 Hz.

The test 3 was repeated on the 4m X-HALE aircraft with sampling rate of 100 Hz in order to verify the ability of the high-pass filtering correction method (Sec. 3.2) to remove the thermal drift while maintaining strain responses in the frequency range of interest. The 4m X-HALE aircraft has bending and torsion strain gage bridges embedded in the wing module 2 presented in Fig. 5. Both measurements were recorded with and without high-pass filtering. During the thermal experiment, impact excitations were done to the wing's tip.

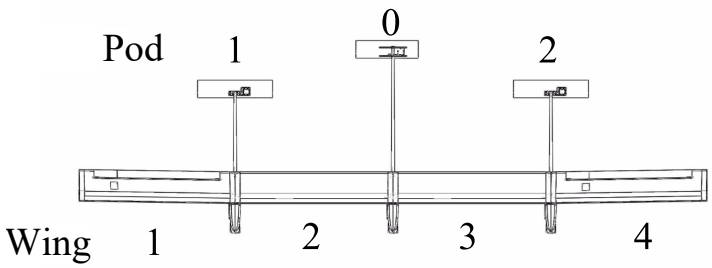

Figure 5: 4m X-HALE aircraft.

3.1.3 Outdoor Thermal Experiment

It consisted of exposing the wing module to natural temperature changes throughout a full day at São José dos Campos, Brazil. The experiment started at 8 AM and ended at approximately 4 PM. Bending, shear and torsion strains, T_{top}, T_{base}, T_{center}, D_{top} and D_{base} were measured throughout the experiment. This experiment was also done on the bi-supported configuration in the 1 m wing module with sampling rate of 1 Hz.

3.2 Thermal Correction Methods

The *functions of temperature correction method* consists of calculating $\varepsilon_{app}\left(\Delta T\right)$ from polynomial functions with two variables coming from least-squares-fit linear regression between temperature inputs and strain response. This method is a simplified version of the one proposed by Moran et al. [8]. In the present work, five input data were tested: T_{top}, T_{base}, $T_{top} - T_{base} = T_{\Delta}$, and its derivatives with respect to time (dT/dt). These were related to indoor and outdoor experimental data in order to find the correction functions. The ones that best predicted $\varepsilon_{app}\left(\Delta T\right)$ were obtained by using T_{Δ} and dT_{Δ}/dt as independent variables and complete indoor experimental strain data (heating and cooling curves) as dependent variable. Functions for bending, shear and torsion bridges were obtained for indoor tests 1, 2 and 3 and the chosen ones were applied to outdoor experimental data in order to assess the effectiveness of this thermal correction in a thermally non-controlled environment.

The *dummy gage correction method* used two CEA 06-250-UW-350 strain gages as dummy gages [9]. They were kept free to expand/contract between two plastic sheets that were loosely attached by one extremity to the top and bottom surfaces of the wing module in the same positions of T_{top} and T_{base} that are near top and bottom bending strain gages. Because of that, constants had to be found to correlate dummy measurements to thermal drift of shear and torsion bridges. Top, bottom and the difference between top and bottom dummy gage data (D_{top}, D_{base} and $D_{top-base}$) were tested to correct bending, shear and torsion bridges.

The *high-pass filtering method* is only recommended for cases where the strain responses of interest are in a known range of frequency that do not include the frequency of thermal drift (approximately 0 Hz). Differently to the MAF cited before, the high-pass filter is applied to the strain measurement in order to remove all quasi-static measurements (including near constant strain due to loads other than temperature). In the X-HALE aircraft, the frequency range of interest is from 0.5 to 20 Hz, allowing for the use of this method. The indoor and outdoor experimental data were filtered in post-processing with a high-pass filter with cutoff frequency of 0.1 Hz. The sampling rate in these experiments was 1 Hz; therefore, the range of response kept in the filtered data is from 0.1 to 0.5 Hz. In order to assure that a similar filter would be suitable for use in the aircraft, a second indoor test was done as described in Section 3.1 with sampling rate of 100 Hz. A 2^{nd} order high-pass digital eliptical filter programmed in Arduino

MEGA 2560 with cutoff frequency of 0.5 Hz was used. A 1^{st} order anti-aliasing analog filter with cutoff frequency of 50 Hz was also added to both filtered and unfiltered data.

3.3 Flight Dynamics Model

To assess if the magnitude of thermal drift and noise obtained for strain gage sensors are small enough to be neglected during X-HALE flight tests, strain responses for Aileron Doublet maneuver with 2° of amplitude were simulated for the 4m X-HALE aircraft.

The flight dynamics model of the 4m X-HALE aircraft is based on the dually-constrained-axis formulation [10, 11], which assumes small deformations. A geometrically-linear three-dimensional FEM model of the aircraft, shown in Figure 6, was built using beam elements, as well as concentrated masses and rigid-body elements. The beam elements have two nodes and twelve degrees of freedom each, and were described by Guimarães Neto et al. [12]. The aerodynamic loads acting on the flexible aircraft are calculated with the doublet-lattice method [13], adjusted with two-dimensional airfoil data based on the XFOIL software [14]. The total aerodynamic loads are the superposition of the loads due to the rigid-body motion and those due to the elastic deformation of the airframe.

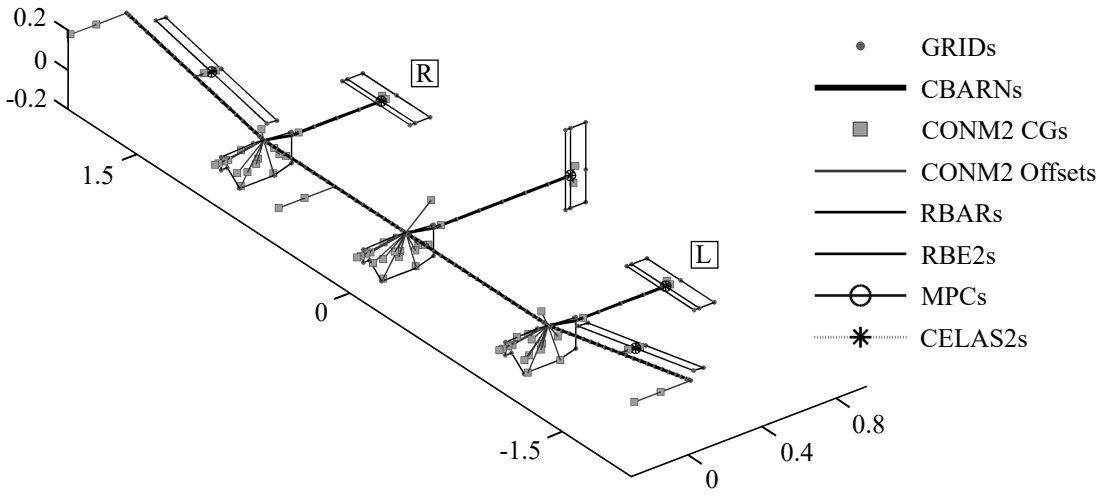

Figure 6: FEM model of 4m X-HALE aircraft.

4 EXPERIMENTAL AND NUMERICAL RESULTS

4.1 Stability over time

The stability test was conducted for approximately 3 hours with no mechanical or thermal loads. Figure 7 presents bending bridge strain data without and with moving average filter (MAF). Similar results were obtained for shear and torsion bridges.

The results showed that strain gage measurement are stable with time. Furthermore, the reduction of measurement noise caused by MAF can be easily seen in Fig. 7. It can also be observed in the reduction of Δ_{strain} (that is given by the subtraction between the maximum and minimum strain measured). The average Δ_{strain} obtained for the three strain gage bridges without moving average filter is approximately 12 $\mu\varepsilon$. it reduces to approximately 3 $\mu\varepsilon$ when the data is filtered. For that reason, the MAF will be used from now on in every data that is only interested in thermal response. Assume the use of MAF in the data unless said otherwise.

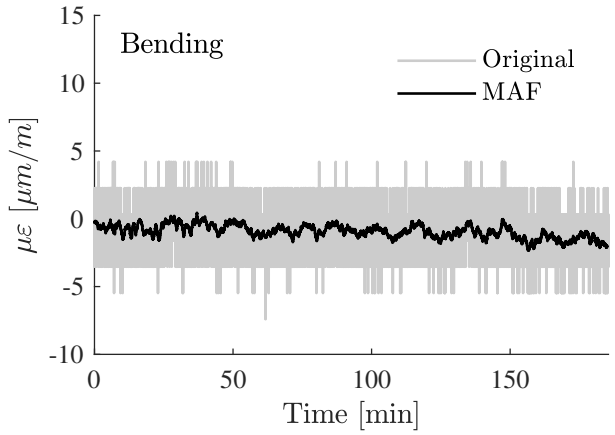

Figure 7: Test of stability over time with duration of 3 hour on X-HALE wing module without and with moving average filtering (MAF) for bending bridge.

4.2 Thermal experiments

Bending, shear and torsion strain measurements due to only thermal loads are presented in Fig. 8 for indoor test 3. The fast initial increase of temperature happened when the lamp was turned on. The three strain gage bridges respond to thermal load almost immediately even though they are in different positions in the wing module. All are embedded between composite layers.

Table 1 shows the maximum temperature (T_{max}) and the average heating rate ($\Delta T/\Delta t$) from the moment that the lamp was turned on to the maximum temperature. It shows the measurements from the three temperature sensors (T_{top}, T_{center} and T_{base}) for each lamp voltage configuration (Tests 1, 2 and 3); maximum strain in module $|\varepsilon_{max}|$, average strain magnitude drop rate ($|d\varepsilon/dt|$) which is the drop in strain measurement calculated from the moment that $|\varepsilon_{max}|$ was measured to the instant that the lamp was turned off (dashed line in Fig. 8(a)) and the strain measured after temperature returns to ambient temperature (0_{end}) are also presented in Table 1 for the three embedded bridges.

Table 1: Temperature and strain data obtained for bending, shear and torsion bridges on three configurations of lamp voltage.

Data	Test 1			Test 2			Test 3		
	Bend.	Shear	Tor.	Bend.	Shear	Tor.	Bend.	Shear	Tor.
$\mid \varepsilon_{max} \mid$ ($\mu\varepsilon$)	44.25	8.69	8.84	50.43	10.94	10.55	47.84	10.02	10.43
$\mid d\varepsilon/dt \mid$ ($\mu\varepsilon/min$)	0.15	0.06	0.10	0.22	0	0.04	0.29	0	0.07
0_{end} ($\mu\varepsilon$)	-4.71	0.43	-0.03	-9.73	-0.94	0.34	-15.26	0.59	2.24
	T_{top}	T_{center}	T_{base}	T_{top}	T_{center}	T_{base}	T_{top}	T_{center}	T_{base}
T_{max} ($^{\circ}C$)	45.45	32.26	35.19	48.88	33.24	36.66	48.88	32.75	36.66
dT/dt ($^{\circ}C/min$)	0.23	0.04	0.07	0.31	0.06	0.11	0.31	0.07	0.09

In general, the differences in lamp voltage caused small variations on T_{max} and $\Delta T/\Delta t$. Even with such small differences between tests, it was observed an increase of $|d\varepsilon/dt|$ related to the increase of $\Delta T/\Delta t$. This also resulted on larger values of 0_{end}. The shear bridge has null $|d\varepsilon/dt|$ because the maximum strain happened when the system was subjected to maximum temperature; therefore, no average strain magnitude drop rate was measured. On the other hand, torsion and bending bridge present $|d\varepsilon/dt|$, which is not expected, knowing that this drop in strain magnitude happens during thermal load increase. Bending bridge is the most sensitive to thermal load which is evidenced by its higher values of $|d\varepsilon/dt|$, 0_{end} and $|\varepsilon_{max}|$.

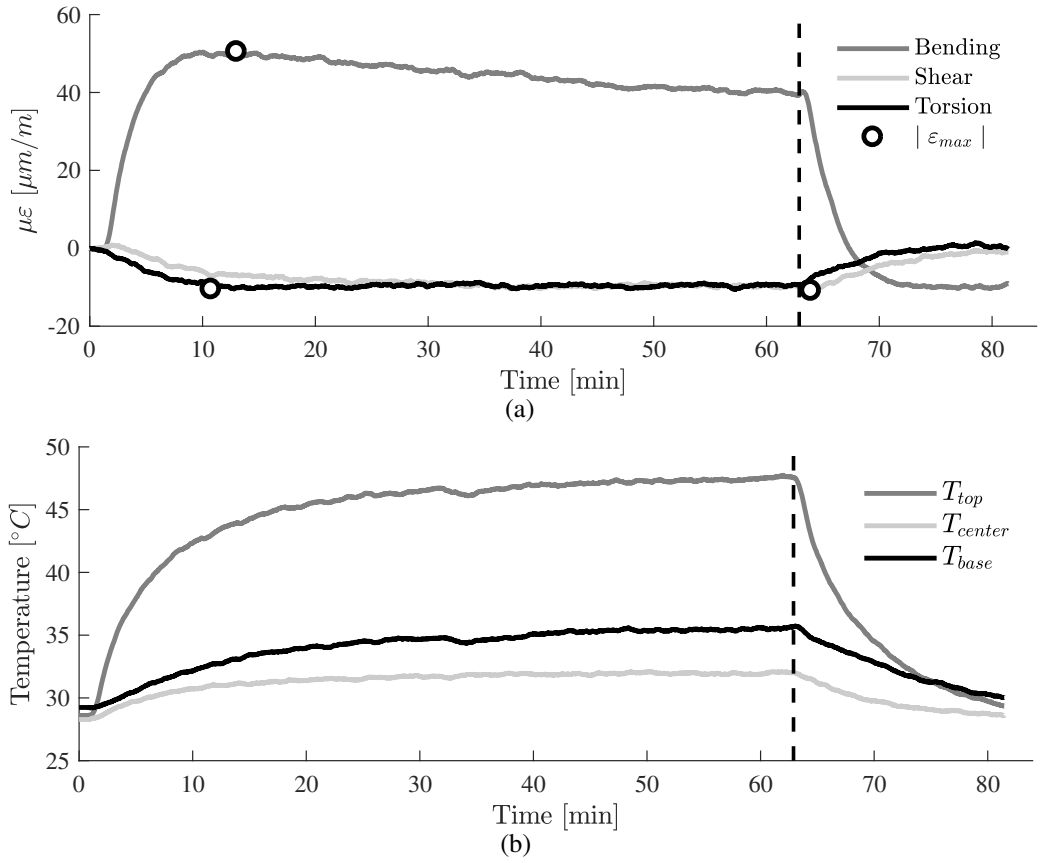

Figure 8: Indoor thermal test 3: a) strain and b) temperature measurements.

Outdoor experiment strain response, as well as T_{top}, T_{center} and T_{base} are presented in Fig. 9. A rapid temperature drop can be seen approximately 4.75 h after experiment start because, from that time on, the wing was no longer exposed to direct sun light, being protected by a shadow.

In order to reduce thermal drift, three correction methods were proposed and compared to original and MAF data: i) functions of temperature, ii) dummy gage and iii) high-pass filtering. All corrections were first tested in indoor experiment data. ε_{max}, ε_{min} and Δ_{strain} of bending, shear and torsion strain with and without corrections are presented in Table 2.

Table 2: Strain measurement data obtained from Test 2 indoor experiment with and without thermal corrections.

Data	Bending			Shear			Torsion		
	ε_{max}	ε_{min}	Δ_{strain}	ε_{max}	ε_{min}	Δ_{strain}	ε_{max}	ε_{min}	Δ_{strain}
Original	53.76	-13.97	67.73	4.37	-15.15	19.52	4.20	-15.41	19.61
MAF	50.43	-10.37	60.80	0.85	-10.94	11.79	1.46	-10.55	12.00
$\varepsilon - f(T)$	8.58	-5.49	14.07	1.95	-1.44	3.38	1.53	-1.61	3.14
$\varepsilon - D_{base}$	42.20	-12.59	54.79	1.02	-6.08	7.10	1.04	-5.93	7.36
$\varepsilon - D_{top}$	2.94	-31.95	34.89	2.73	-4.84	7.57	1.61	-2.79	4.40
$\varepsilon - D_{top-base}$	4.72	-19.95	24.67	4.14	-4.77	8.91	2.63	-2.69	5.33
F_{strain}	0.61	-0.21	0.82	0.09	-0.22	0.31	0.10	-0.21	0.31

The functions $f(T)$ obtained from indoor test 2 were chosen for functions of temperature correction due to their higher coefficient of determination (R^2) and better correction results in all embedded bridges. Figure 10 shows the strain data (ε), the strain obtained from $f(T)$ and the results after correction ($\varepsilon - f$) for bending bridge. This correction was effective in reducing

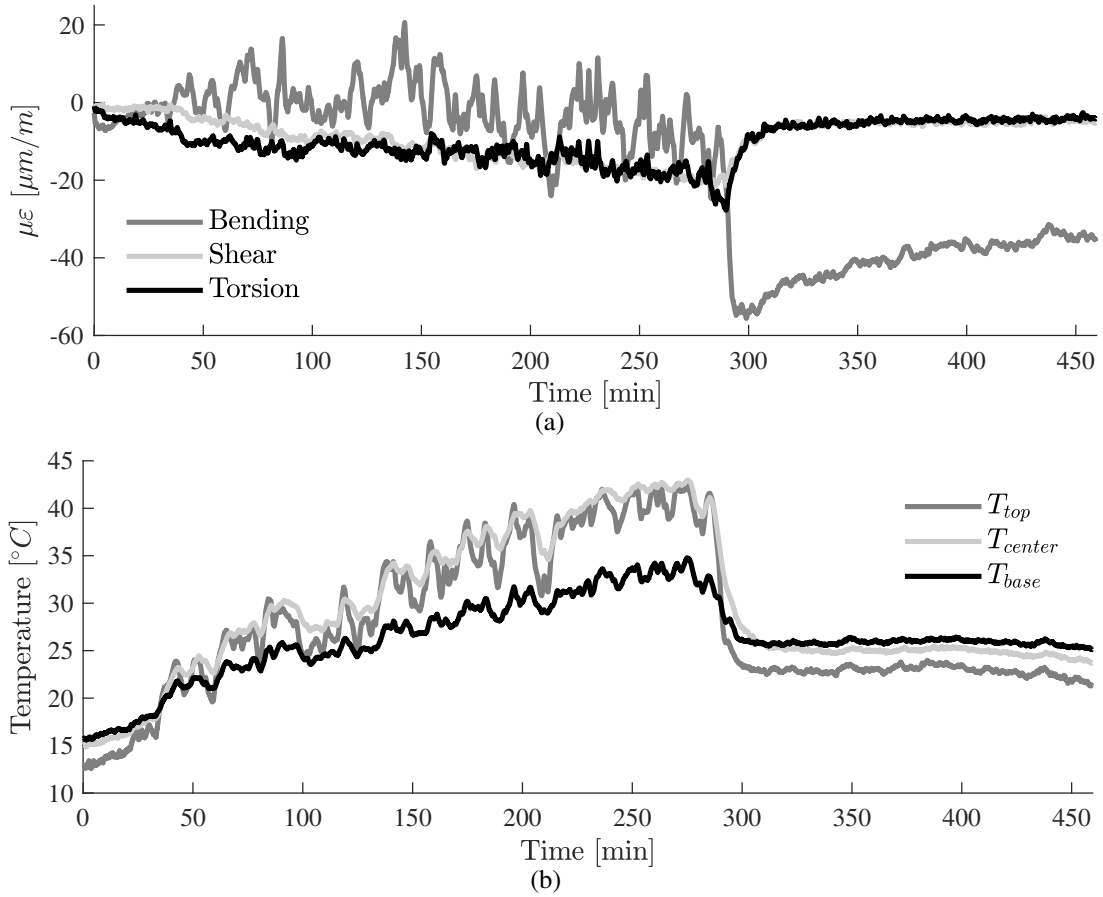

Figure 9: Outdoor thermal test: a) strain and b) temperature measurements.

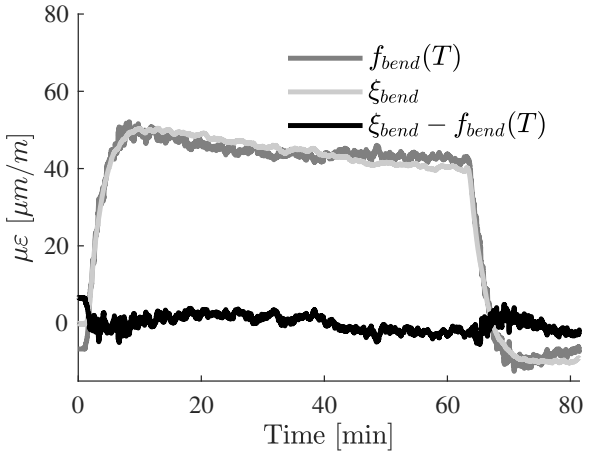

Figure 10: Functions of temperature correction applied to bending bridge strain data of indoor test 2.

thermal drift on indoor experiment strain data. When comparing the corrected curve to MAF data, it was observed a reduction of 77%, 71% and 74% of Δ_{strain} for bending, shear and torsion bridges respectively.

The use of only D_{top}, D_{base} and $D_{top-base}$ on the Dummy gage correction are compared in Fig. 11 for bending bridge. For this case the best correction was obtained when using $D_{top-base}$ with a reduction of 55% and 29% of Δ_{strain} when compared to corrections using D_{base} and D_{top}. For shear and torsion bridges, the best correction was obtained when using D_{base} and D_{top} respectively, resulting in reductions of 40% and 63% of Δ_{strain} when comparing corrected

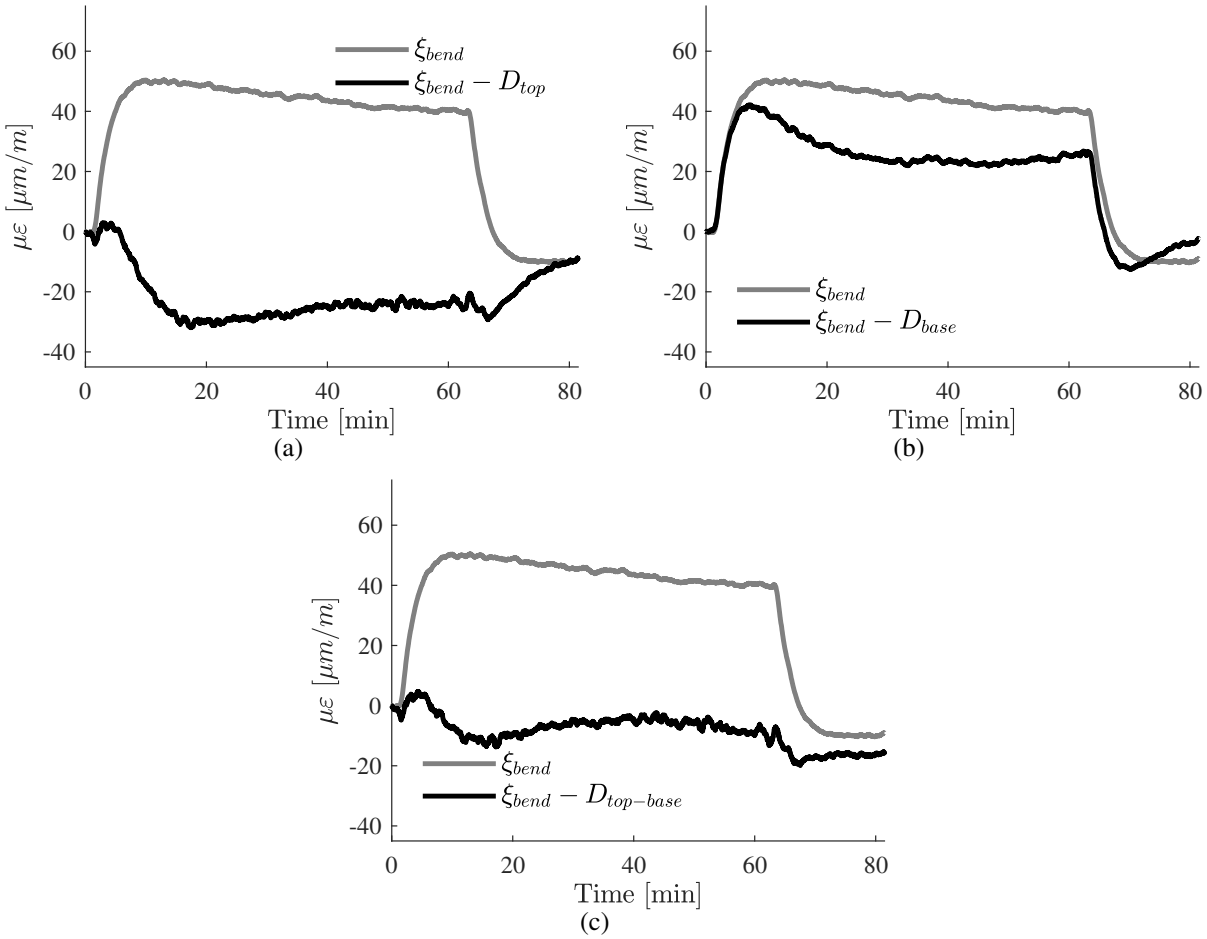

Figure 11: a) D_{top}, b) D_{base} and c) $D_{top-base}$ dummy corrections applied to bending bridge strain data of indoor test 2.

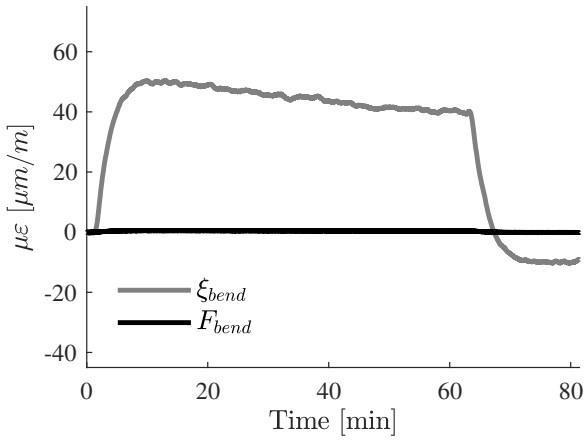

Figure 12: High-pass filter correction applied to bending bridge strain data of indoor test 2.

curves to MAF data.

Figure 12 shows that the high-pass filtering correction (F_{bend}) was able to completely remove the strain measurement due to thermal load in the indoor experiment data. When comparing the corrected curve to MAF data, it was observed a reduction of 99% of Δ_{strain} for bending bridge and 97% for shear and torsion bridges.

The corrections configurations with best results for functions of temperature and dummy gage

correction (when applied to indoor experiments) were used for outdoor experiment correction and the results are presented in Figs. 13 and 14. The outdoor experiment correction with high-pass filtering is presented in Fig. 15. A good thermal correction of outdoor experiment data was not achieved for the two first correction methods for any of the three strain bridges, while high-pass filtering was successful in removing thermal drift from the three measurements.

When comparing the corrected curve obtained by function of temperature to MAF data, an increase of approximately 24% of Δ_{strain} was observed for bending and 15% for shear bridge. On the other hand, this correction was able to achieve a reductions of 6% of Δ_{strain} for torsion bridge.

When comparing the dummy gage correction curve to the MAF data, an increase of approximately 32% and 44% of Δ_{strain} were observed for bending and torsion bridge. The shear bridge presented higher increase of 160%.

For the high-pass filtering correction, a reduction of 99% of Δ_{strain} was observed for bending and 98% for shear and torsion bridges when comparing the data with thermal correction and with MAF.

The existence of $|\Delta\varepsilon/\Delta t|$ during temperature increase (observed also on outdoor experiment) suggests that the strain measurements not only depends on the temperature itself, but also on the heating/cooling rate and the exposure time to each temperature. This makes the $\varepsilon_{app}\left(\Delta T\right)$ much harder to predict, explaining why a less controlled environment experiment result in less effective function of temperature and dummy gage thermal corrections. On the other hand, the high-pass filtering method does not aim to predict $\varepsilon_{app}\left(\Delta T\right)$, but only to remove all low frequency responses. Therefore, an increase in the complexity of the thermal system does not affect the performance of this method.

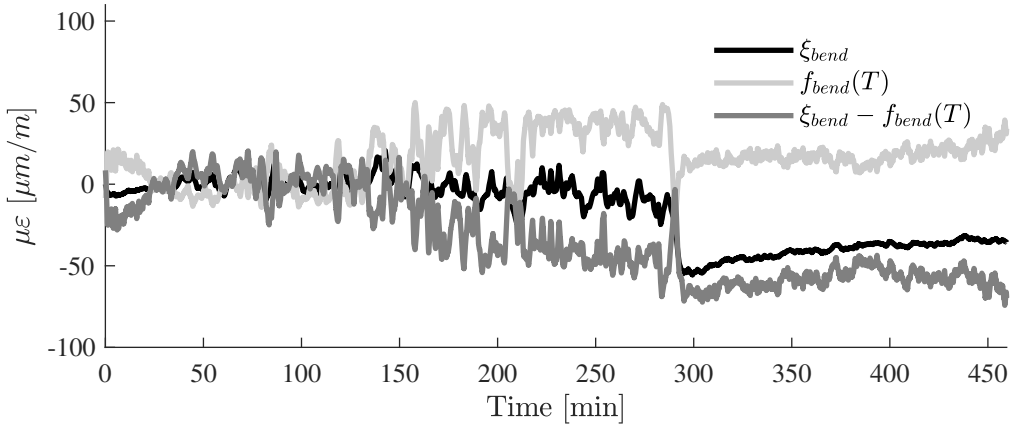

Figure 13: Functions of temperature correction applied to bending bridge strain data of outdoor experiment.

Table 3: Strain measurement data obtained from outdoor experiment with and without thermal corrections.

Data	Bending			Shear			Torsion		
	ε_{max}	ε_{min}	Δ_{strain}	ε_{max}	ε_{min}	Δ_{strain}	ε_{max}	ε_{min}	Δ_{strain}
Original	24.2	-59.01	83.21	5.14	-24.14	29.28	1.92	-31.41	33.33
MAF	20.64	-55.61	76.25	-0.01	-21.41	21.40	0.04	-27.73	27.76
$\varepsilon - f(T)$	20.40	-74.25	94.65	1.89	-22.71	24.60	0.03	-25.92	25.95
$\varepsilon - D$	72.94	-27.82	100.76	17.90	-37.72	55.62	-0.02	-39.89	39.87
F_{strain}	0.28	-0.69	0.97	0.09	-0.31	0.40	0.08	-0.38	0.46

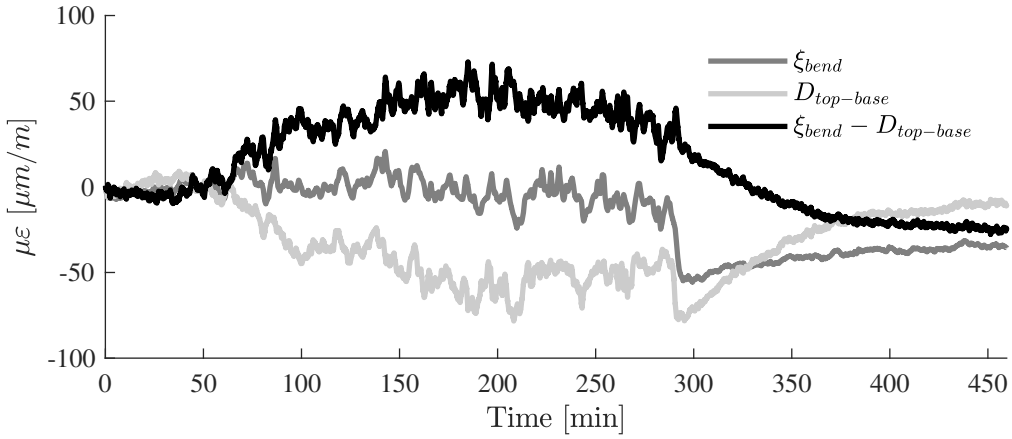

Figure 14: Dummy correction applied to bending bridge strain data of outdoor experiment.

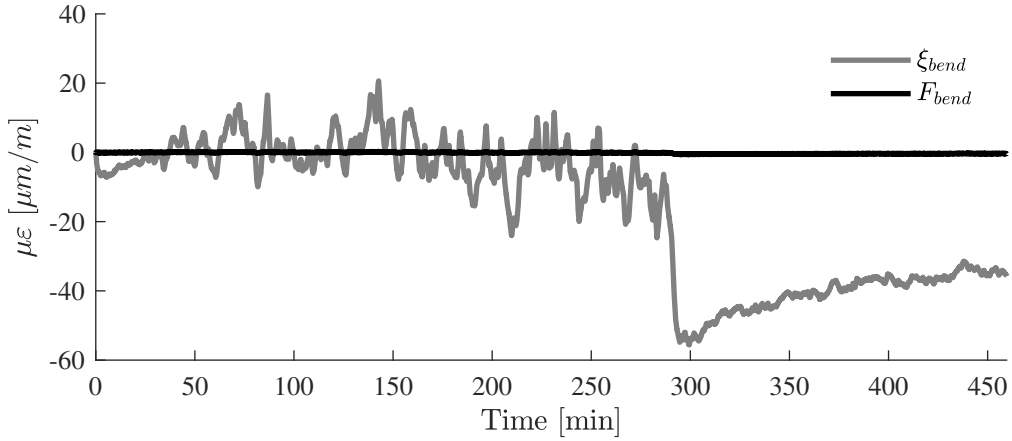

Figure 15: High-pass filter correction applied to bending bridge strain data of outdoor experiment.

Flight experiments of X-HALE aircraft are expected to last for a maximum of 10 min, and the acquisition system will be stabilized in the zero strain point prier to each flight. Therefore, thermal corrections need to be effective for only 10 min and not the 8 hours of outdoor experiment presented. Because of this, 10 min windows were chosen on outdoor experiment data and stabilized on the zero strain point at the beginning of the window in order to better compare the correction methods. Three windows were chosen based on the three maximum Δ_{strain} obtained for bending bridge and are presented in Fig. 16. The comparison between original strain data (ε_{strain}), with moving average filter (MAF), with functions of temperature correction (Function), dummy gage correction (Dummy) and high-pass filtering (F_{strain}) are presented in Figs. 17, 18, 19 and Table 4.

The high-pass filtering correction was more effective in reducing thermal drift in every time window for all three strain gage bridges. The second best correction method was the dummy gage correction that presented the second smaller Δ_{strain} in all windows for bending bridge and window 3 for shear bridge.

4.3 Simulated strain for flight maneuver

The commanded deflections u_R and u_L, related to right and left elevator and aileron command surfaces (according to Fig. 6), are presented in Fig. 20 for aileron doublet input with 2° of amplitude. For all surfaces, positive deflection means trailing edge downwards. Simulated strain due to maneuver is presented in Fig. 21, measured on the two center wing modules of X-HALE aircraft (Fig. 6) for the cases of flight speed of 12, 16 and 20 m/s.

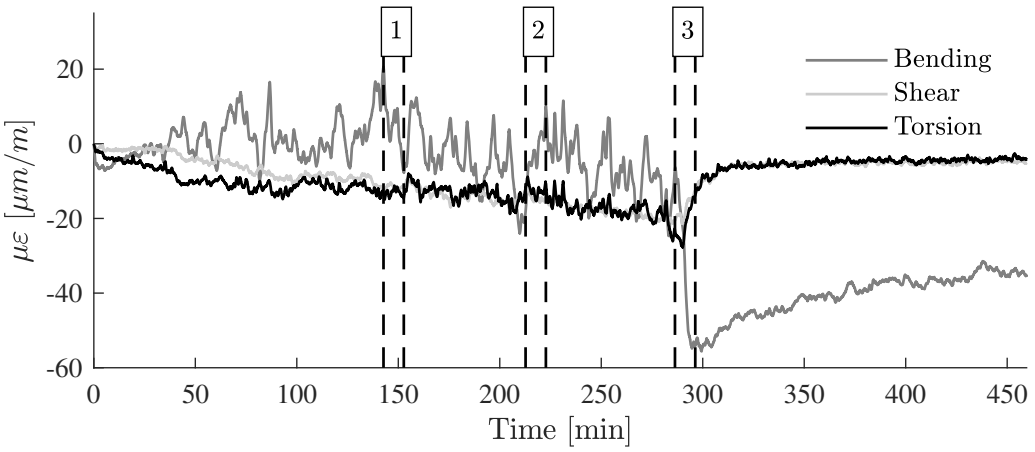

Figure 16: Outdoor experiment and chosen 10 min windows. Filtered strain data.

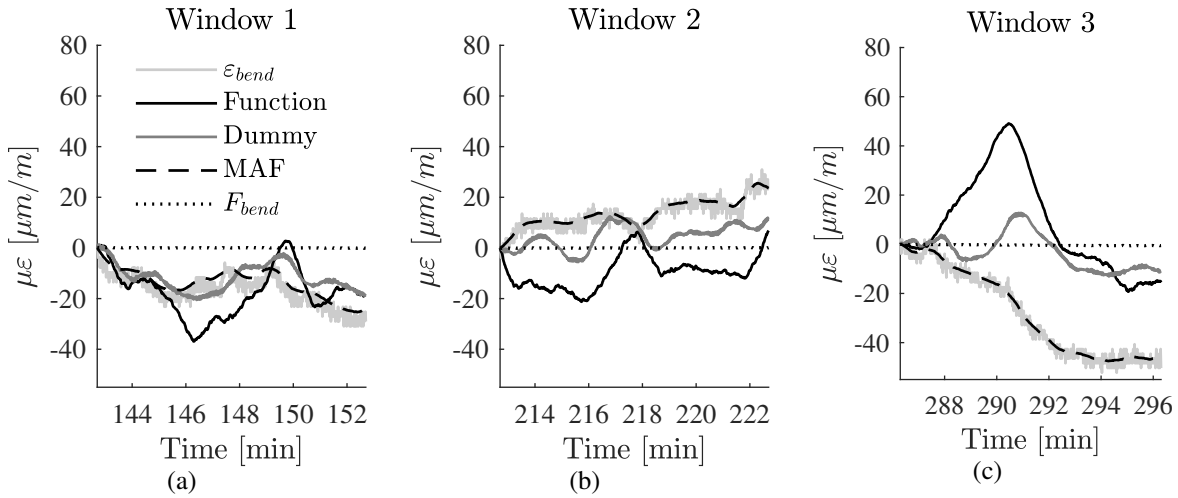

Figure 17: Bending bridge data with and without thermal corrections on 10 min time windows a) 1, b) 2 and c) 3.

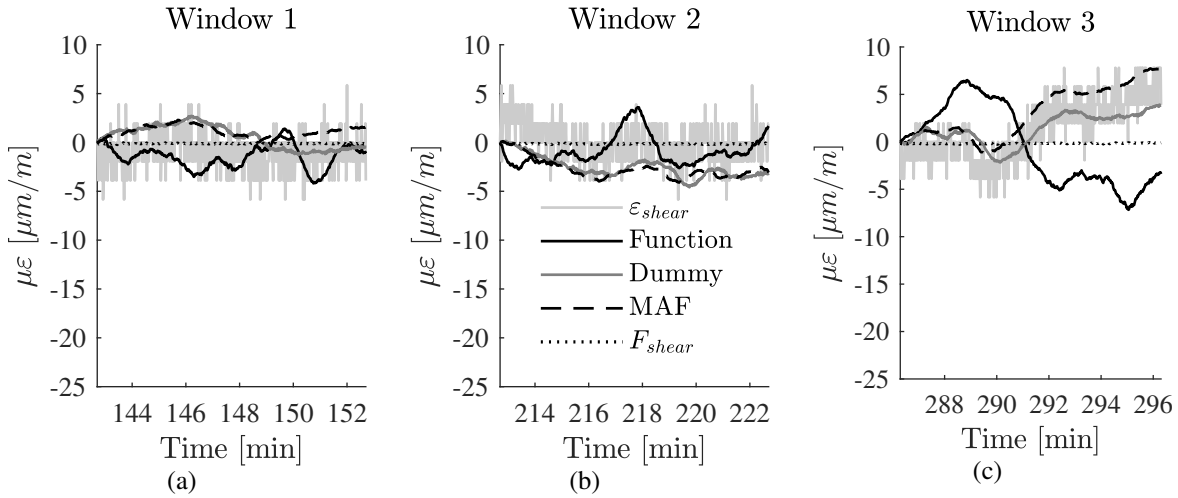

Figure 18: Shear bridge data with and without thermal corrections on 10 min time windows a) 1, b) 2 and c) 3.

In the numerical model, the strain measurement is null when the aircraft has zero structural loads. On experimental tests, strain gages will be set to zero prior to each flight when the aircraft is at rest. Therefore, the analysis will be done focusing on the Δ_{strain} obtained during maneuver that is presented in Table 5.

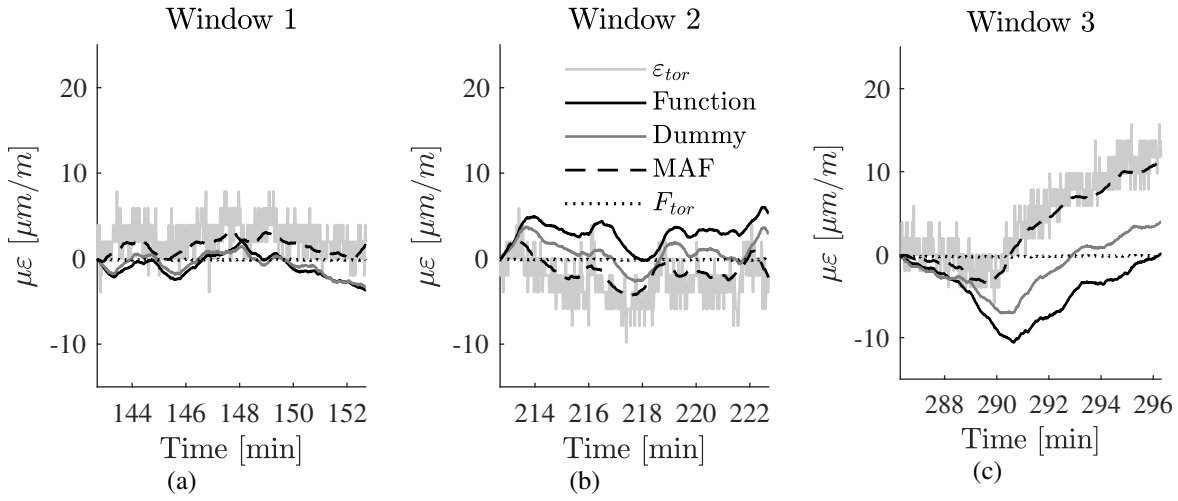

Figure 19: Torsion bridge data with and without thermal corrections on 10 min time windows a) 1, b) 2 and c) 3.

Table 4: Δ_{strain} of 10 min time windows of outdoor experiment with and without thermal corrections.

Data	Window 1			Window 2			Window 3		
	$\Delta_{bend.}$	Δ_{shear}	$\Delta_{tor.}$	$\Delta_{bend.}$	Δ_{shear}	$\Delta_{tor.}$	$\Delta_{bend.}$	Δ_{shear}	$\Delta_{tor.}$
Original	30.96	11.71	11.77	34.83	11.71	15.69	54.18	13.66	21.57
MAF	25.35	2.38	3.73	25.58	4.25	6.55	47.49	9.02	14.83
Function	39.67	5.60	5.67	28.08	6.35	6.27	68.41	13.68	10.67
Dummy	21.86	3.98	4.70	18.03	4.75	6.41	25.89	6.09	11.01
F_{strain}	0.36	0.23	0.22	0.40	0.21	0.26	0.63	0.27	0.31

Table 5: Δ_{strain} of simulated strain results in response to aileron doublet inputs.

Flight Speed	Bending		Torsion		Shear	
	Right	Left	Right	Left	Right	Left
12 m/s	28.38	27.95	10.39	10.22	5.27	5.18
16 m/s	52.77	54.08	12.04	11.55	6.08	5.89
20 m/s	78.25	80.85	15.04	15.35	7.68	7.79

The smallest Δ_{strain} obtained for bending bridge with high-pass filtering correction (of 0.36 on Window 1 of Table 4) corresponds to 1% of the smallest Δ_{strain} of bending bridge for flight maneuver. Similarly, shear and torsion smallest Δ_{strain} with high-pass filtering (Window 2 and 1 respectively) represent 4% of shear bridge and 2% for torsion bridge for aileron doublet maneuver.

The second smallest Δ_{strain} obtained for bending bridge (of 18.03) with Dummy gage correction on Window 2 of Table 4 corresponds to 65% of the smallest Δ_{strain} of bending bridge for flight maneuver. Similarly, shear and torsion second smallest Δ_{strain} of 2.38 and 3.73 respectively, obtained for filtered data of Window 1 represent 46% of shear bridge and 36% for torsion bridge for aileron doublet input.

The high-pass filter is the best thermal correction method of the ones tested in the present work, being able to remove thermal drift of strain gage sensors subjected to simple and complex temperature variations. However, all slow strain responses will be lost with this method.

For other applications in which the expected strain measurements are not as small as in the case of X-HALE aircraft, dummy gage correction can be used, knowing that it was able to reduce

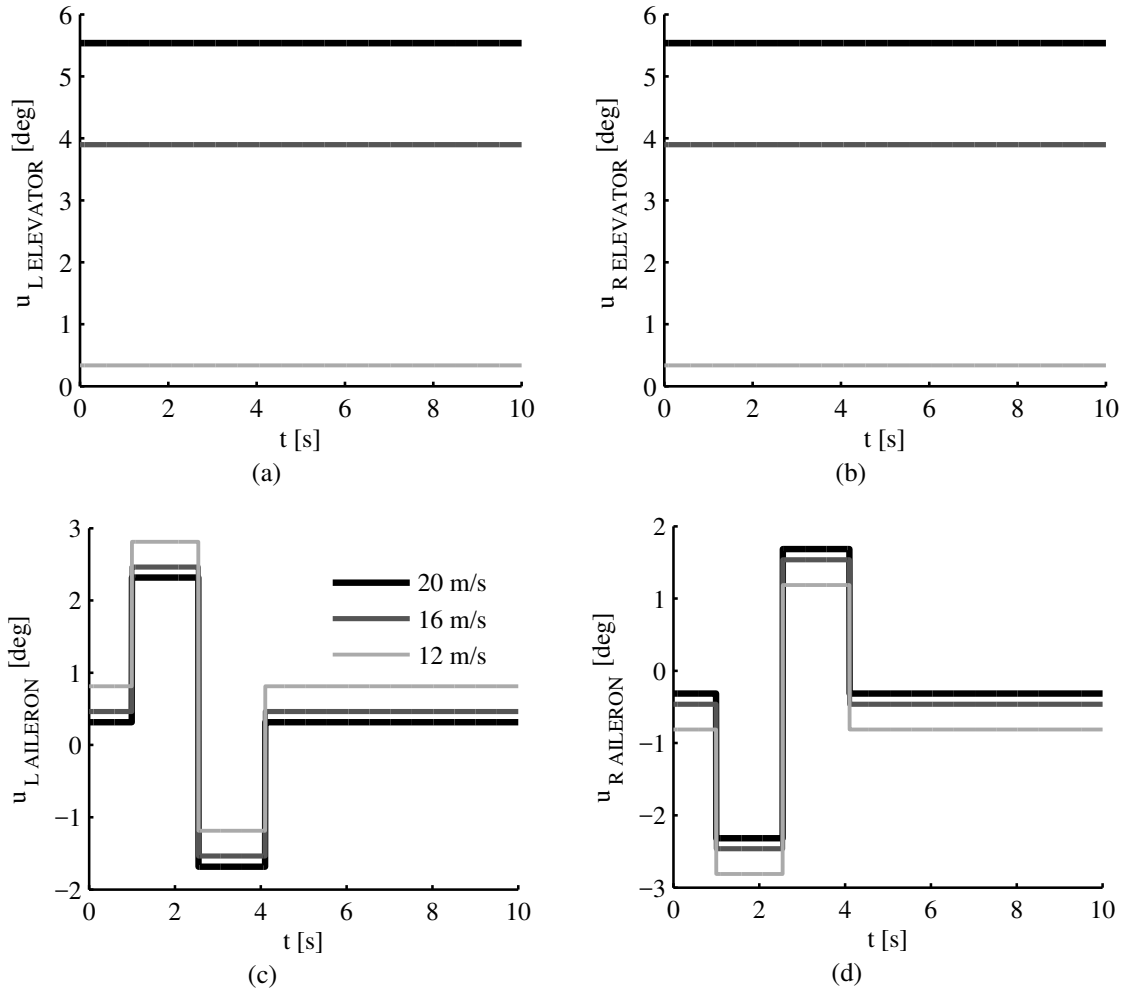

Figure 20: Commanded deflection of a) left elevator, b) right elevator, c) left aileron and d) right aileron in aileron doublet input.

thermal drift in most of the time windows analyzed.

For cases where the temperature variation is expected to happen in a more controlled environment, both functions of temperature and dummy gage correction methods can be used.

4.4 High-pass filtering in X-HALE aircraft

In order to verify the ability of the high-pass filtering correction method to remove the thermal drift while maintaining strain responses in the frequency range of interest, the indoor thermal test was repeated in the 4m X-HALE full aircraft with sampling rate of 100 Hz. Bending measurement with and without high-pass filtering during heating and cooling are presented in Figs. 22 and 25. T_{top} and T_{base} for each of these sections are presented in Figs. 23 and 26. The peaks in Figs. 22 and 25 are the strain responses due to impact excitation. These excitations during heating and cooling are shown in detail in Figs. 24 and 27. The curves presented do not have MAF. Therefore, the relation between base noise and strain measurement is what is expected to happen during flight tests. Similar responses were obtained for torsion bridge.

Once again, the high-pass filtering method was able to remove thermal drift from measurement. The excitation response, on the other hand, was kept mostly unchanged. The frequency and amplitude of bending and torsion due to excitation are the same for the cases with and without

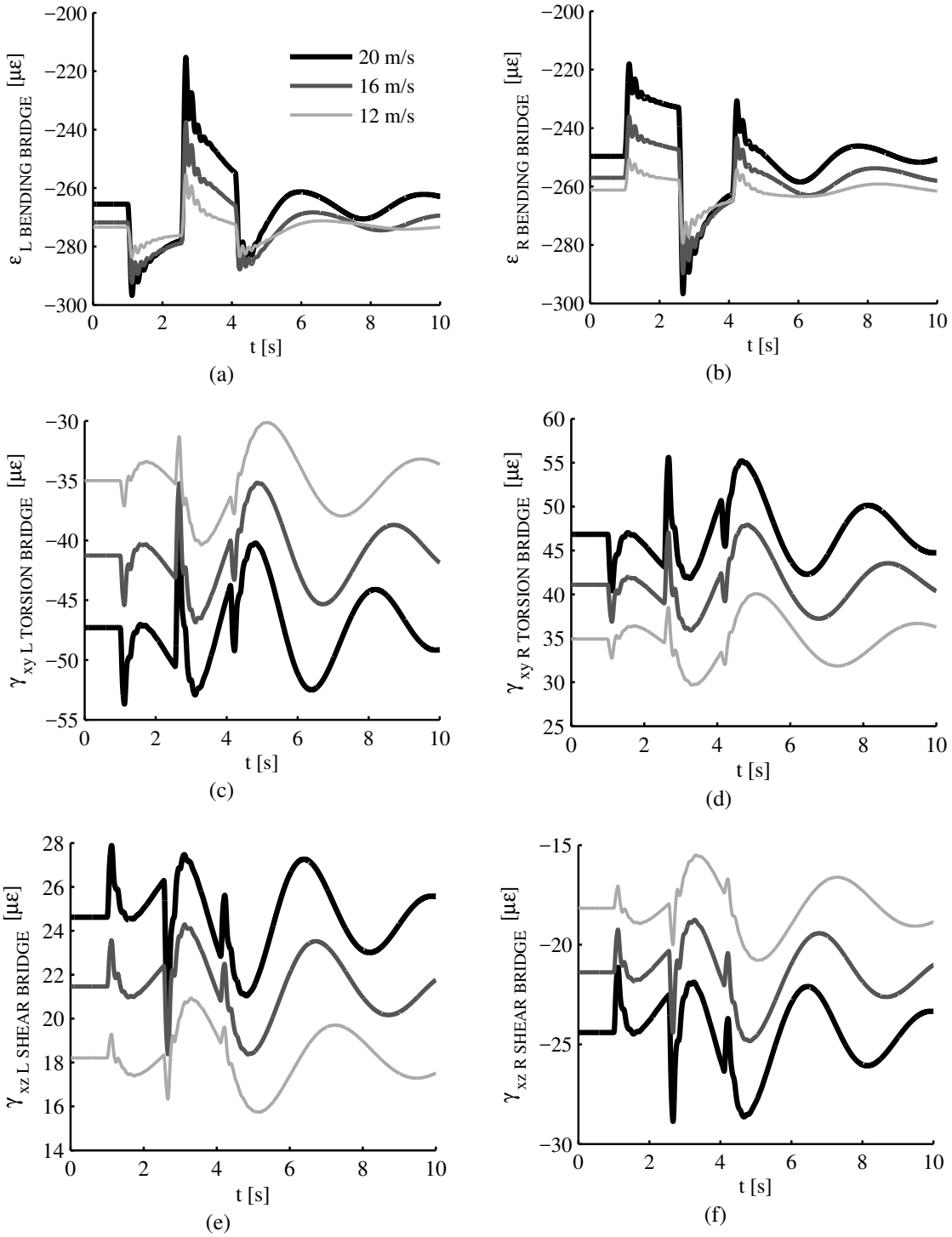

Figure 21: Bending (a and b), shear (c and d) and torsion (e and f) strains in aileron doublet input.

high-pass filtering. Therefore, this method was able to create strain measurement suitable for use in control systems in the X-HALE aircraft.

5 CONCLUSION

This paper presented results of thermal tests on strain gage sensors embedded between composite layers of the X-HALE aircraft wing. These tests were done with the goal to determine which thermal correction method is able to create corrected strain measurements, in real time,

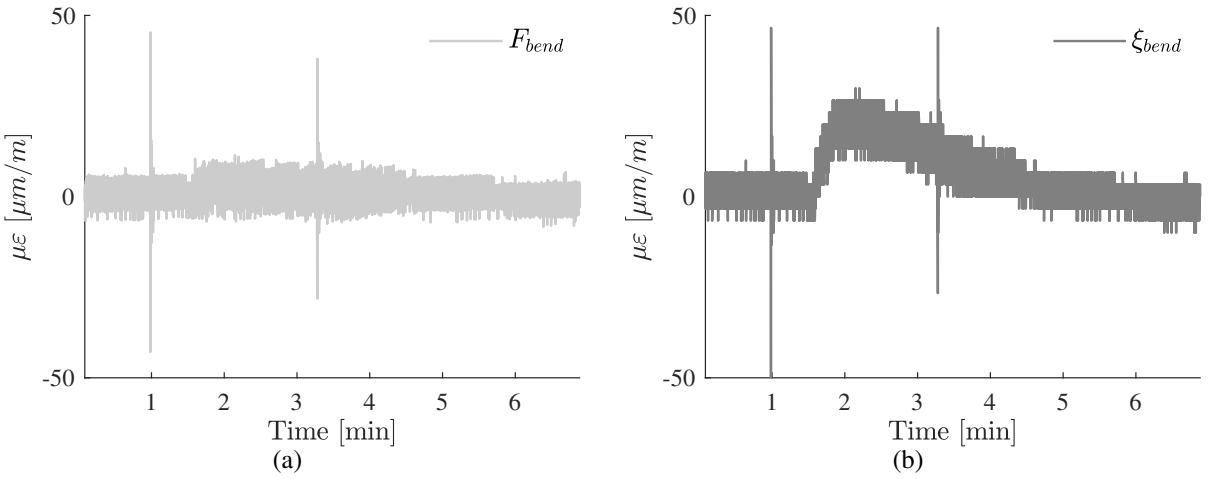

Figure 22: Bending strain a) with and b) without high-pass filtering correction during heating (sampling rate of 100 Hz).

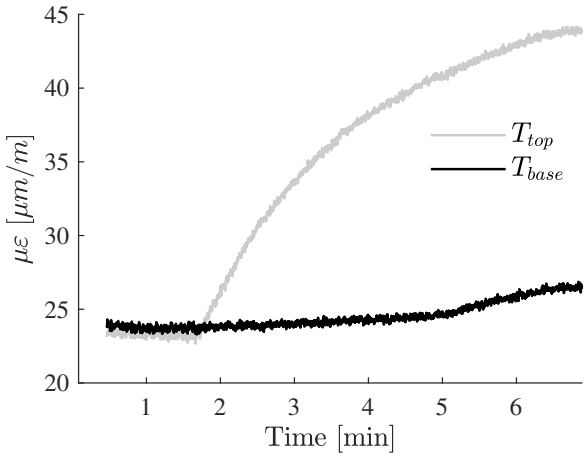

Figure 23: Temperature measurement of indoor experiment during heating (sampling rate of 100 Hz).

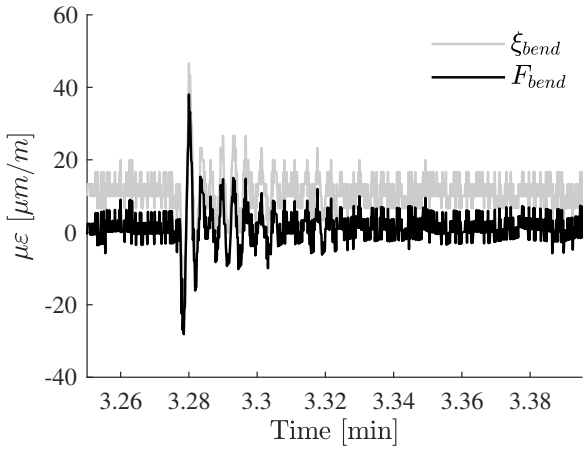

Figure 24: Bending strain due to impulse excitation during heating (sampling rate of 100 Hz).

to be used in control systems. Thermal tests in indoor and outdoor environments were done on a 1 m X-HALE wing module. Thermal drifts of 50.43 $\mu\varepsilon$ were measured when the system was under $48.88°C$. Three correction methods were tested on both indoor and outdoor experiment data: functions of temperature, dummy gage and high-pass filtering. All three correction methods were effective in removing thermal drift of indoor experiment data. On the other hand,

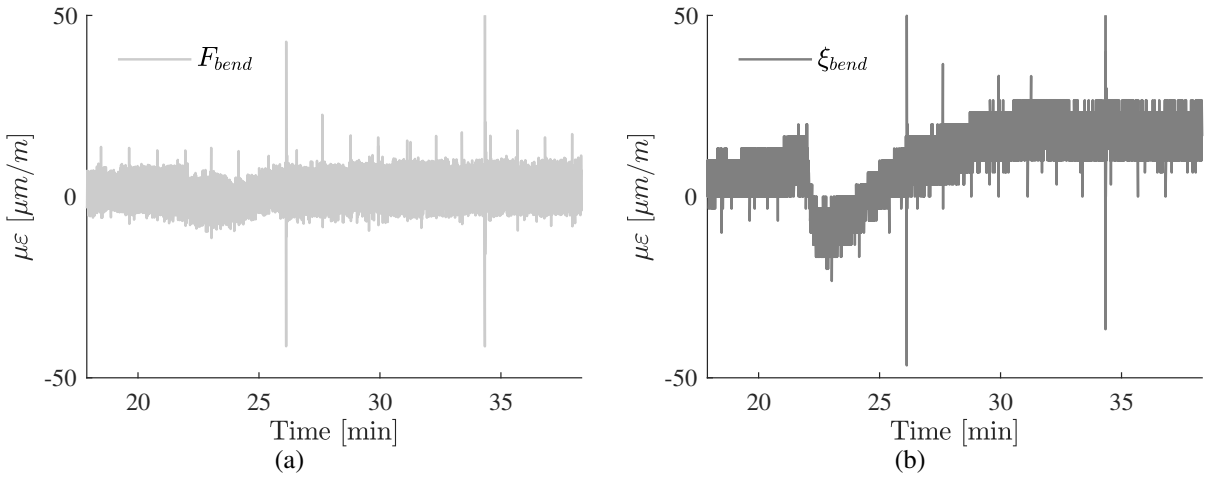

Figure 25: Bending strain a) with and b) without high-pass filtering correction during cooling (sampling rate of 100 Hz).

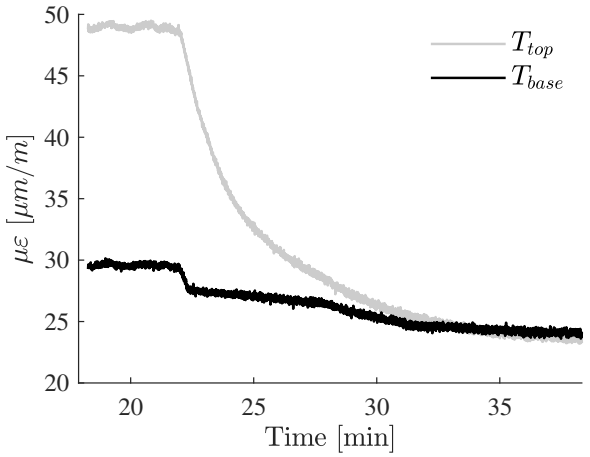

Figure 26: Temperature measurement of indoor experiment during cooling (sampling rate of 100 Hz).

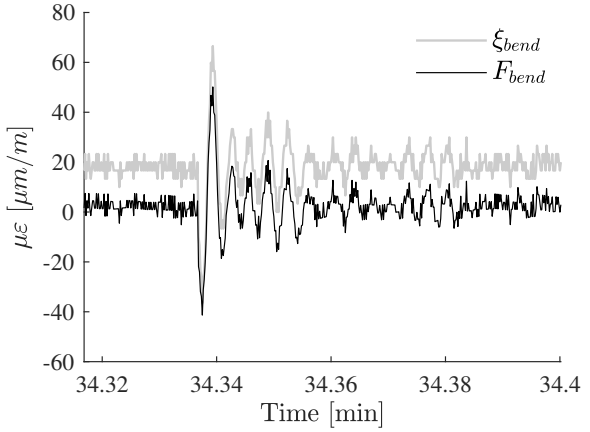

Figure 27: Bending strain due to impulse excitation during cooling (sampling rate of 100 Hz).

only the high-pass filtering method was successful in the outdoor experiment. The results were compared to data with moving average filter (MAF) on time windows of 10 min (time similar to the duration of an X-HALE flight). The best results were obtained for high-pass filtering method, which was able to completely remove thermal drift from measurements. This method was applied in an indoor thermal test done on the full 4m X-HALE aircraft, with the addition of impact excitations on the aircraft's wing tip. This method was proved to be suitable for

the present application, being able to remove thermal drift while maintaining responses in the frequency range of interest.

ACKNOWLEDGMENT

This work has been supported by FINEP and EMBRAER under the research project Advanced Studies in Flight Physics, contract number 01.14.0185.00; and by CNPq, Conselho Nacional de Desenvolvimento Científico e Tecnológico - Brasil.

6 REFERENCES

[1] Anderson Jr., J. D. (2010). *Fundamentals of aerodynamics*. Tata McGraw-Hill Education.

[2] Pedlow, G. W. and Welzenbach, D. E. (1998). *The CIA and the U-2 Program, 1954-1974*. DIANE Publishing.

[3] Cesnik, C. E. S., Senatore, P. J., Su, W., et al. (2012). X-hale: A very flexible unmanned aerial vehicle for nonlinear aeroelastic tests. *AIAA journal*, 50(12), 2820–2833.

[4] Patil, M. J. and Hodges, D. H. (2006). Flight dynamics of highly flexible flying wings. *Journal of Aircraft*, 43(6), 1790–1799.

[5] Di Sante, R., Donati, L., Troiani, E., et al. (2014). Reliability and accuracy of embedded fiber bragg grating sensors for strain monitoring in advanced composite structures. *Metals and Materials International*, 20(3), 537–543.

[6] Richards, W. L. (1996). A new correction technique for strain-gage measurements acquired in transient-temperature environments. Tech. rep., National Aeronautics and Space Administration - NASA.

[7] Jones, J. R. (2015). Properties of the x-hale aeroelastic test vehicle (x-hale atv). Tech. rep., University of Michigan.

[8] Moran, M. E., Gregory, S. D., Robinson, J. R., et al. (2010). Active temperature differential compensation for strain gage based sensors. US Patent 7,647,837.

[9] Micro-Measurements, V. (2007). Strain gage thermal output and gage factor variation with temperature. *Strain Gages and Instruments*, 35–47.

[10] Guimarães Neto, A. B., Silva, R. G. A., Paglione, P., et al. (2016). Formulation of the flight dynamics of flexible aircraft using general body axes. *AIAA Journal*, 54(11), 3516–3534. doi:10.2514/1.J054752.

[11] Guimarães Neto, A. B. (2014). *Flight dynamics of flexible aircraft using general body axes: a theoretical and computational study*. Ph.D. thesis, Instituto Tecnológico de Aeronáutica, São José dos Campos, Brazil. Thesis (PhD in Aeronautical and Mechanical Engineering).

[12] Guimarães Neto, A. B., Silvestre, F. J., Cardoso-Ribeiro, F. L., et al. (2017). Validity of the assumption of small deformations in aircraft with different levels of structural flexibility. In *Proceedings of the International Forum on Aeroelasticity and Structural Dynamics*, IFASD Paper 080. Como, Italy.

[13] Albano, E. and Rodden, W. P. (1969). A doublet-lattice method for calculating lift distributions on oscillating surfaces in subsonic flows. *AIAA Journal*, 7(2), 279–285. doi: 10.2514/3.5086.

[14] Drela, M. (1989). XFOIL: An analysis and design system for low reynolds number airfoils. In T. Mueller (Ed.), *Low Reynolds Number Aerodynamics*, vol. 54 of *Lecture Notes in Engineering*. Springer Berlin Heidelberg. ISBN 978-3-540-51884-6, pp. 1–12. doi: 10.1007/978-3-642-84010-4_1.

COPYRIGHT STATEMENT